Myosin Va Movements in Normal and *Dilute-Lethal* Axons Provide Support for a Dual Filament Motor Complex

P.C. Bridgman

Department of Anatomy and Neurobiology, Washington University School of Medicine, St. Louis, Missouri 63110

Abstract. To investigate the role that myosin Va plays in axonal transport of organelles, myosin Va–associated organelle movements were monitored in living neurons using microinjected fluorescently labeled antibodies to myosin Va or expression of a green fluorescent protein–myosin Va tail construct. Myosin Va–associated organelles made rapid bi-directional movements in both normal and *dilute-lethal* (myosin Va null) neurites. In normal neurons, depolymerization of microtubules by nocodazole slowed, but did not stop movement. In contrast, depolymerization of microtubules in *dilute-lethal* neurons stopped movement. Myosin Va or synaptic vesicle protein 2 (SV2), which partially colocalizes with myosin Va on organelles, did not accumulate in *dilute-lethal* neuronal cell bodies because of an anterograde bias associated with organelle transport. However, SV2 showed peripheral accumulations in axon regions of *dilute-lethal* neurons rich in tyrosinated tubulin. This suggests that myosin Va–associated organelles become stranded in regions rich in dynamic microtubule endings. Consistent with these observations, presynaptic terminals of cerebellar granule cells in *dilute-lethal* mice showed increased cross-sectional area, and had greater numbers of both synaptic and larger SV2 positive vesicles. Together, these results indicate that myosin Va binds to organelles that are transported in axons along microtubules. This is consistent with both actin- and microtubule-based motors being present on these organelles. Although myosin V activity is not necessary for long-range transport in axons, myosin Va activity is necessary for local movement or processing of organelles in regions, such as presynaptic terminals that lack microtubules.

Key words: myosin Va • actin • microtubules • organelles • *dilute-lethal*

THE transport requirements of neurons are particularly demanding because of their highly polarized and complex shapes. Transport of organelles to their proper locations in neurons may require the cooperative interaction between microtubule- and actin-based motors (Langford, 1995). Fast axonal transport of organelles requires microtubule-based motor activity (reviewed in Hirokawa, 1993). However, if neurons are grown without microtubules, organelles are still transported at reduced rates within the shorter axon-like processes that form (Morris and Hollenbeck, 1995). Actin-based motors (myosins) may be responsible for this residual component of transport in the absence of microtubules. Myosin Va is a likely candidate (Evans et al., 1997, 1998; Tabb et al., 1998).

Myosin Va is the product of the *dilute* locus in mice (Mercer et al., 1991; Cheney et al., 1993). *Dilute* mutations affect both skin and hair color and, in severe alleles, produce neurological symptoms that lead to death (Mercer et al., 1991). Myosin Va is an unconventional myosin that has biochemical properties compatible with a transport function in vivo (Espreafico et al., 1992; Cheney et al., 1993; Wolenski et al., 1995). Recent data indicate that the myosin Va heavy chain can interact directly with a microtubule-based transport motor, the kinesin heavy chain (Huang et al., 1999). Organelles destined for transport to the cell periphery may therefore contain both microtubule and actin-based motors, possibly arranged as a single motor complex.

Myosin Va associates with vesicles in cultured neurons (Evans et al., 1997). A population of vesicles enriched in myosin Va has been purified from brain (Evans et al., 1998). A substantial fraction of these (~90 nm) vesicles have myosin Va tightly bound to the surface and are colabeled with markers for synaptic vesicles. When activated, the vesicles can drive the movement of actin filaments in vitro. A function-blocking antibody to myosin Va stopped the movement. Synaptic vesicle proteins also associate with myosin Va in a calcium-dependent manner (Prekaris and Terrian, 1996). Myosin V is bound to squid axoplasm-derived organelles that move on both microtubules and

Address correspondence to Dr. Paul C. Bridgman, Department of Anatomy and Neurobiology, Box 8108, Washington University School of Medicine, 660 S. Euclid Ave., St. Louis, MO 63110. Tel.: (314) 362-3449. Fax: (314) 747-1150. E-mail: bridgmap@thalamus.wustl.edu

actin filaments (Kuznetsov et al., 1992; Tabb et al., 1998). There, antibodies to squid myosin V inhibited organelle movements on actin. Furthermore, *dilute-lethal* mice show abnormal distributions of smooth endoplasmic reticulum in Purkinje cell neurons (Takagishi et al., 1996). While organelles move on actin filaments in intact growth cones (Evans and Bridgman, 1995), the motor responsible for this movement is unknown. We hypothesize that myosin Va contributes to movement of vesicles in intact neurons. We test that hypothesis here.

Myosin Va may play an essential role in long-range melanosome movement and localization. Myosin Va binds to melanosomes (Provance et al., 1996; Nascimento et al., 1997; Wu et al., 1997) and has also been implicated in *Xenopus* melanophore movement (Rogers and Gelfand, 1998). In the absence of myosin Va, melanosomes concentrate abnormally in the perinuclear region of melanocytes, suggesting a role in melanosome transport (Provance et al., 1996; Wei et al., 1997; Wu et al., 1997). Recently, however, the importance of myosin Va motor activity for melanosome long-range transport has been challenged by results that favor a capture model for melanosome localization in melanocytes (Wu et al., 1998). In this model, melanosome localization is determined by bi-directional microtubule-dependent melanosome movements coupled with actomyosin Va–dependent capture of melanosomes in the periphery of the cell. The minimum requirement for the capture mechanism is the tethering of melanosomes to actin filaments. Although a capture mechanism does not require actin-based transport, melanosome movement appears to be at least partially dependent on myosin Va activity (Wu et al., 1998). This suggests that short-range melanosome movements in peripheral regions of dendrites may be myosin Va dependent. It is unknown if myosin Va may act as a tether or mediate primarily short-range movements within defined regions of neurons. Therefore, we also tested this hypothesis.

These two hypotheses were tested with a set of experiments on neurons cultured from *dilute-lethal* mice, which do not express myosin Va. The goals were to: (a) test the requirement of myosin Va motor activity for movement of myosin Va–associated organelles in axons, (b) determine if myosin Va–associated organelles can move under conditions where microtubules have been eliminated, and (c) determine if the capture paradigm proposed for myosin Va–mediated melanosome localization can explain the localization and dynamics of myosin Va–associated organelles in neurons.

Myosin Va motor activity was found to be unnecessary for organelle movement in axons. Instead, microtubules were found to be required for the rapid, bi-directional myosin Va–associated organelle movements that were observed in both normal and *dilute-lethal* axons. Thus, myosin Va appears to be mostly a passive passenger on organelles during normal microtubule-mediated long-range axonal transport.

Unexpectedly, myosin Va–associated organelles did not concentrate in cell bodies of neurons of *dilute-lethal* mice. Instead, myosin Va–associated organelles accumulated peripherally in axon areas rich in microtubule ends, due in part because of a bias toward anterograde transport. Thus, the apparent incompatibility with the capture model presented for melanocytes may be due more to differences in the net balance of anterograde and retrograde transport than to an incompatibility with a myosin Va–dependent tethering. These results support the hypothesis that cooperation between the two filament systems (microtubules and actin filaments) is necessary for localization and trafficking of organelles in vertebrate axons and their terminations. Myosin Va–mediated transport appears to be necessary for proper short-range transport or processing of organelles in microtubule-deficient regions such as nerve terminals. This may include a role in local transport to vesicle fusion sites or "loading" myosin Va–associated organelles destined for retrograde transport onto microtubule tracks in peripheral regions of the neuron. It also suggests that in different regions of neurons either microtubules or actin filaments may predominate as the essential transport tracks.

Materials and Methods

Cell Culture

Explant and dissociated cultures of superior cervical ganglion (SCG)[1] neurons were prepared from embryonic rats (E19) or postnatal mice (P0) as described previously (Dailey and Bridgman, 1993; Evans et al., 1997). For microinjection and gene gun experiments, cells were plated on substrates coated with 0.1–0.2 mg/ml polyornithine followed by laminin (16 μg/ml). Microinjection was performed 1–3 d after plating. For cultures grown in nocodazole or latrunculin, the drug was added from stock solutions prepared in DMSO directly to the plating medium (unless indicated), and then exchanged for fresh medium + drug every 48 h. The final DMSO concentration did not exceed 0.01%. Latrunculin A was used at a concentration of 0.1 μg/ml (Spector et al., 1989). Cytochalasin E was used at a concentration of 20 μg/ml (Morris and Hollenbeck, 1995). Nocodazole was used at a concentration of 3.3 μg/ml unless indicated.

SCG neurons from *dilute-lethal* mice were more sensitive to nocodazole than cells from rats or heterozygous mice. Less than 10% of the cells plated directly in medium containing nocodazole-developed processes after 3 d in culture (compared with ~70% in controls). Therefore, a modified approach was used. SCG neurons from *dilute-lethal* and heterozygous littermates were plated in normal medium and grown for either 4 or 16 h. The cultures were then switched to medium containing nocodazole. Two different concentrations of nocodazole were used to depolymerize microtubules from neurites. Cultures grown for 4 h received 0.1 μg/ml, while cultures grown for 16 h received 0.15 μg/ml nocodazole.

Immunoblots

An affinity-purified antiserum to rat myosin Va was used on immunoblots of homogenized whole brain to identify *dilute-lethal* ($d^{l\text{-}20J}/d^{l\text{-}20J}$) P0 mouse pups. The methods were the same as previously described (Evans et al., 1997).

Antibody Microinjection

The antiserum used for microinjection was made against a maltose binding protein—rat myosin Va tail fusion protein. The myosin Va peptide corresponded to amino acids 1005–1830 of the mouse myosin Va sequence, which includes part of the rod and the entire globular tail (Cheney et al., 1993). The affinity purification and specificity of the antiserum has been described previously (Evans et al., 1997). An IgG fraction of the affinity-purified antiserum was used for conjugation with indocarbocyanine (Cy3). The conjugation was carried out according to instructions provided by the manufacturer of the dye (BDS). The conjugate was separated from free dye on a G25 column and eluted in injection buffer (100 mM KCL, 10 mM Na_2HPO_4, pH 7.2). The concentration of dye compared with

1. *Abbreviations used in this paper:* BDS, biological detection systems; Cy3, indocarbocyanine; GFP, green fluorescent protein; iu, intensity units; SCG, superior cervical ganglion; SV2, synaptic vesicle protein 2.

protein was estimated from absorbance at 556 and 280 nm; the ratio was 5:1. The resulting protein solution was concentrated threefold using a Centriprep-30 concentrator. The activity was tested by immunofluorescence labeling of cultured SCG neurons. The distribution of label was identical to that obtained with the nonconjugated purified antiserum. Before micropipette filling, the solution was centrifuged for 15 min at maximum speed in a microcentrifuge. An Eppendorf microinjection system equipped with Femtotips was used for pressure microinjection. Considering the appearance in phase contrast and ability to retain dye, ~60–80% of the rat cells survived the injection processes. Mouse neurons were more difficult to inject and so most microinjection experiments used rat neurons. Healthy cells were imaged 15 min to 5 h after microinjection unless otherwise indicated.

Biolistics

A rat myosin Va cDNA clone containing the coil–coil and globular tail, but lacking the IQ repeats and motor domain (Evans et al., 1997) was inserted into a green fluorescent protein (GFP) vector (Clontech) and amplified in bacteria. Purified plasmid DNA was used for transfection. 1- or 1.6-μm gold particles were coated with 2 μg DNA per mg gold according to the manufacturer's instructions. SCG cultures were transfected with a hand-held Helios gene gun (Bio-Rad Laboratories) using a pressure of 70–80 psi 1–3 d after plating.

Fluorescence Imaging of Live Cells

Neurons microinjected with myosin Va-Cy3 antibodies, or expressing the GFP-myosin Va tail construct, were imaged at 37°C on an inverted microscope (Olympus Corp.) with a 100× 1.4 NA lens (Nikon Inc.), unless otherwise indicated. Before imaging, the cultures were switched to a Hepes-based culture medium (+ or − the appropriate drug). A 100-W mercury arc lamp was used for illumination. The light was attenuated with a neutral density filter (25% transmittance) and shuttered between exposures. Images were collected using a cooled, slow scan CCD (C250; Photometrics) containing a 512 × 512 pixel chip (thinned, back illuminated; Tektronix Inc.). The images were binned (2 × 2). Exposures were 0.25 or 0.5 s at 6- or 5-s intervals.

Immunofluorescence

Cultures were fixed for 20–30 min with a warm (37°C) solution of 4% paraformaldehyde (EM grade; EM Sciences) in 0.1 M cacodylate buffer, pH 7.4, containing 10 mM $CaCl_2$ and 10 mM $MgCl_2$. Cells were permeabilized with 0.1% saponin or 0.1% Triton in the same buffer for 30 min. They were incubated with blocking solution (8 mg/ml BSA, 5% goat serum, 0.5% fish gelatin) for 20–30 min, and then labeled with primary antibodies diluted in a 1/5 dilution of the blocking solution for 1 h. The anti–rat myosin Va affinity purified antiserum was used at a concentration of 0.5 μg/ml. The SV2 mAb (gift of Dr. K. Buckley) was used at a 1/200 dilution. The anti–synaptophysin mAb (Sigma Chemical Co.) was used at a 1/1,000 dilution. Secondary antibody (minimal species cross-reacting antibodies; Jackson Immunochemicals) incubations were for 45–60 min; dilutions ranged from 1/200 (FITC) to 1/1,000 (Cy3). An antifade agent (Vectashield) was used to minimize photobleaching during imaging.

To determine the degree of colocalization of fluorescent spots, the 16-bit images were converted to 8 bits and superimposed in two different colors. They were scored as "colocalized" if their fluorescent area overlapped and the peak brightness of the SV2 or synaptophysin staining was at least 20% of the brightness of the myosin Va staining. Although this may underestimate the degree of association between the two labels, it prevents the possibility of scoring spots for colocalization that show apparent association due to fluorescence filter bleed-through.

For quantitation of intensity, values were taken directly from flat field–corrected 16-bit images and were expressed in relative intensity units (iu) with a maximum possible value of 65,000. For each comparison, the same exposure time and excitation light intensity were used. Absolute values of intensity units obtained in different comparisons depended on the intensity of the excitation light and exposure time, which was varied between experiments.

Analysis of Moving Fluorescent Spots

The movement of either Cy3-labeled antibody or GFP-myosin Va (tail) fluorescent spots was analyzed with the following method. Time-lapse images were adjusted for optimal contrast, and then played in series using the movie tool available in either Isee (Inovision Corp.) or Iplab Spectrum (Scanalytics). Sequences from thin neurites with relatively few clearly visible spots were selected for analysis. This allowed us to follow the same spot between time points because most spots moved in predictable trajectories within a single focal plane. The sequences were zoomed (2×) and played forward, and then in reverse so that moving spots could be selected and followed over multiple frames. For each frame, a mark was placed over the center of an individual spot on a clear acetate overlay on the computer monitor screen. Spots that could not be followed for at least four frames (elapsed time of 15 or 18 s) were not used in the final analysis. This limited the analysis to ~30% of the spots that appeared to move in a sequence. The distance between marks was measured in millimeters, and then converted to micrometers using a calibration slide (Leica Inc.) imaged with the same optics and CCD detector, and then displayed on the monitor. The number of time points analyzed for individual spots was highly variable (4–18). For comparison purposes, the average rate of displacement was defined as the displacement that occurred between the first and fifth time point divided by the total elapsed time (20 or 24 s). The maximum rate was defined as the largest displacement between two time points divided by the time interval.

Electron Microscopy

Photoconversion. Methods were modified from published methods (Lubke, 1993; Kazca et al., 1997). Cultures grown on aclar coverslips containing neurons that had been microinjected with the anti–myosin Va-Cy3–conjugated antibody were returned to the incubator and allowed to grow for 30–90 min. Cells were fixed with a warm mixture of 0.25% glutaraldehyde and 0.32% paraformaldehyde in 0.1 M sodium cacodylate buffer, pH = 7.4, containing 10 mM $CaCL_2$ and $MgCL_2$. The cells were reidentified by fluorescence and phase microscopy and the images recorded. The cultures were preincubated with cold 1.4 mg/ml DAB (Sigma Fast DAB; Sigma Chemical Co.) in phosphate buffer for 15 min. After exchange with fresh cold solution, the microinjected cells were irradiated using a 100-W mercury arc lamp on an inverted microscope (Olympus Corp.). A 25×, 0.75 NA oil immersion lens with high transmittance (Leica Inc.) was used for the irradiation. Irradiation times were varied from 15 to 35 min. Fluorescence and bright field observations were periodically made to check for photobleaching and appearance of a dark brown reaction product. Darkening was detected by 15 min, but photobleaching was not complete until ~35 min. For controls, cells that were not microinjected, but on the same coverslip, were irradiated for the same times in fresh DAB solution. Cells were further fixed with 2.5% glutaraldehyde for 30 min. They were post-fixed with 3% osmium tetroxide for 1 h. Before dehydration and embedding, the cells were stained with 1% uranyl acetate dissolved in 1% sodium acetate for 1 h. The areas containing the photoconverted cells were cut from the larger aclar coverslip to allow identification before thin sectioning. The coverslip piece was flat embedded. Once the coverslip was removed from the polymerized resin, the cells could be identified by phase contrast microscopy using the recorded images as guides, and then further trimmed for sectioning.

Immunoelectron microscopy of cultured cells. After microinjection and recovery in the incubator, cells were fixed and images were recorded as described above. Cells were treated with 1 mg/ml sodium borohydride in PBS for 20 min. The cells were permeabilized with 0.05% filipin in PBS for 30 min. They were incubated with the antibody blocking solution for 30 min, followed by incubation with 6 nm colloidal gold conjugated to an anti–rabbit antibody overnight at 4°C.

Immunoelectron microscopy of brain slices. The procedure was modified from that described by Mrini et al. (1995). Mice were perfused with 0.25% glutaraldehyde + 4% paraformaldehyde in cacodylate buffer, pH 7.4 (+ 2 mM $CaCl_2$). The brain was removed and immersed in the same fixative for at least 4 h. The cerebellum was dissected free and embedded in agar for vibratome sectioning. 50-μm sections were cut. The sections were treated with freshly made 1 mg/ml sodium borohydride in PBS for 20 min. They were equilibrated with 35% sucrose + 14% glycerol in PBS. The sections were frozen for 15 s in isopentane cooled with liquid nitrogen and thawed in PBS. This was repeated once. The sections were incubated for 2 h with PBS containing 0.1% saponin. They were incubated for 2 h in block solution containing (freshly made) 0.1% saponin. The incubation was changed to block solution without saponin and continued for another 30 min. They were incubated overnight at room temperature with the primary antibodies (1/2,000 antimyosin Va; 1/200 anti–SV2 mAb) in a 1/5 dilution of the block. The incubation was continued at 4°C for another 48 h. After washing with PBS on rocker for 1 h, the sections were incubated overnight on a

rocker with gold-conjugated antibodies diluted 1/50 in a 1/5 dilution of the block. The incubation was continued at 4°C overnight. The sections were washed on a rocker for 1 h in PBS. They were fixed with 2.5% glutaraldehyde in PBS for 1 h. They were postfixed with osmium-potassium ferricyanide (Harris and Stevens, 1989) and stained en block with 1% uranyl acetate for 1 h. They were dehydrated and embedded using standard procedures.

Quantitative Analysis of Presynaptic Area and Synaptic Vesicle Density

EM images were digitized using a high-resolution scanner (Agfa Duoscan). The areas of presynaptic terminals were determined by tracing the perimeter of terminals in Iplab Spectrum. The area in pixels was converted to square micrometers using the calibration bars printed on the EM negatives. Because the number of mitochondria in terminals were highly variable and could influence the calculation of synaptic vesicle density, their area was also determined and subtracted from the measured terminal area for the calculation of synaptic vesicle density. The numbers of synaptic vesicle profiles were counted and the density calculated from the corrected terminal area.

Results

Localization of Myosin Va-Cy3–labeled Antibodies After Microinjection into Cultured Neurons

Initially, a series of antibody concentrations and injection pressures were tested in microinjection experiments. It was determined that at a minimal injection pressure (<4 psi) and low antibody concentrations (<2 mg/ml) small bright myosin Va-Cy3 spots appeared in superior cervical ganglion neurons. The size and distribution of these spots were consistent with previous results using myosin Va antibody staining on fixed SCG neurons (Evans et al., 1997; our unpublished results). The bright spots were not apparent immediately after injection, but appeared at the earliest time point (15 min) for time-lapse observations after injection (Fig. 1 A) and persisted at least 16 h (longest time after injection of observation). Higher concentrations of antibody (4 mg/ml) or injection pressures produced much larger bright spots (Fig. 1, B and C). The small bright spots were highly dynamic, while the large bright spots never made rapid movements [but in neurites did make slow (0.28 ± 0.08 μm/min, $n = 15$) retrograde movements]. The absence of larger spots from the dimmer microinjected cells combined with the differences in dynamics suggests that the large spots represented aggregates of the smaller spots formed by antibody cross-linking.

SCG neurons cultured from *dilute-lethal* mice grow and extend neurites normally in culture (Evans et al., 1997). Neurons injected ($n = 8$) with the different concentrations of the antibody showed only a diffuse distribution of fluorescence in cell bodies and neurites (Fig. 1, D and E). The lack of bright spots in *dilute-lethal* neurons indicates that the spots are likely to result from specific interactions with myosin Va–containing structures rather than nonspecific antibody aggregation or sequestration.

Dynamics of Myosin Va-Cy3 Antibody in Neurites

The rapid movements of individual small bright spots observed in neurites of rat (21 cells) or heterozygous (d^v/d^l) mouse (nine cells) SCG neurons injected with low concentrations of antibody at reduced pressures were measured and analyzed in several different ways. Most frequently, during a 20-s time period, ~10% of the spots moved and the remaining were stationary. Movement of spots was bidirectional; spots sometimes paused or transiently reversed direction, but usually made progress either towards or away from the cell body (Fig. 2, A and B). For analysis, movements away from the cell body are designated with positive values, while movements toward the cell body are indicated by negative values. Among the 40 spots selected

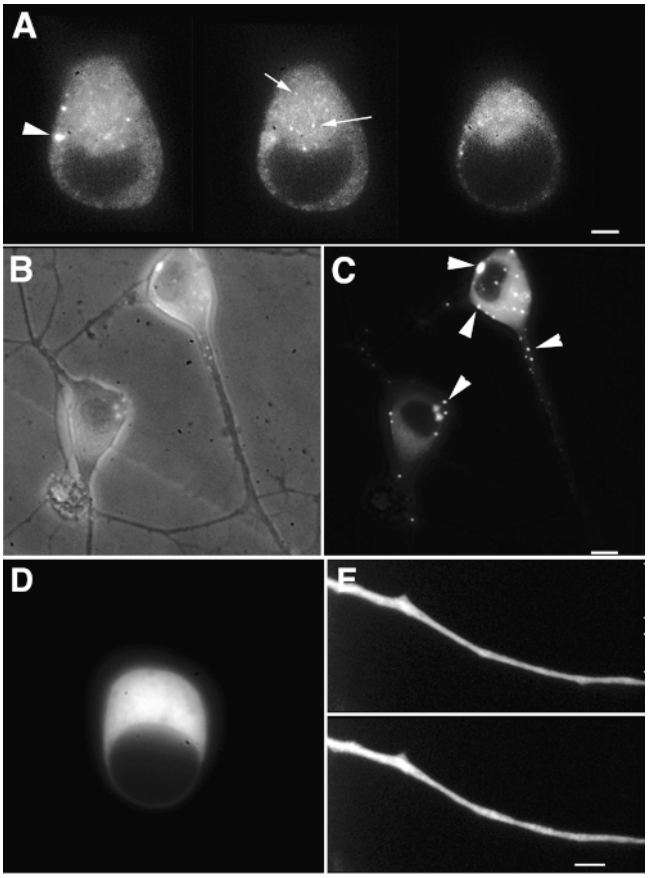

Figure 1. Microinjection of myosin Va-Cy3 affinity purified antiserum into normal (A–C) and *dilute-lethal* (D and E) neurons produces genotype-specific results. (A) High magnification images taken at three different focal planes through a rat neuron injected with a low concentration (<2 mg/ml) of the Cy-3–conjugated antiserum. One bright spot (arrowhead) is visible, but smaller, dimmer spots (arrows) predominate. (B) A lower magnification superimposed image of fluorescence on a phase contrast image of the rat SCG neurons reveals the neurites. (C) Fluorescence image from the same cells in B showing the bright spots (arrowheads) that form upon microinjection of higher concentrations (4 mg/ml) of the antiserum into normal SCG neurons. The upper neuron has brighter diffuse fluorescence and a greater number of spots indicating that more antiserum was injected. Large bright spots may represent aggregates of the small spots induced by antibody cross-linking. Microinjection of antibodies into neurons from heterozygous mice gave the same result. (D) An SCG neuron cultured from a *dilute-lethal* mouse shows only diffuse fluorescence in the cell body (D) and neurite (E) when microinjected with the Cy-3–conjugated anti–myosin Va antiserum. (E) Two images of a neurite separated by 5 min. Bars: (A) 3 μm; (B and C) 6.5 μm; (D and E) 3 μm.

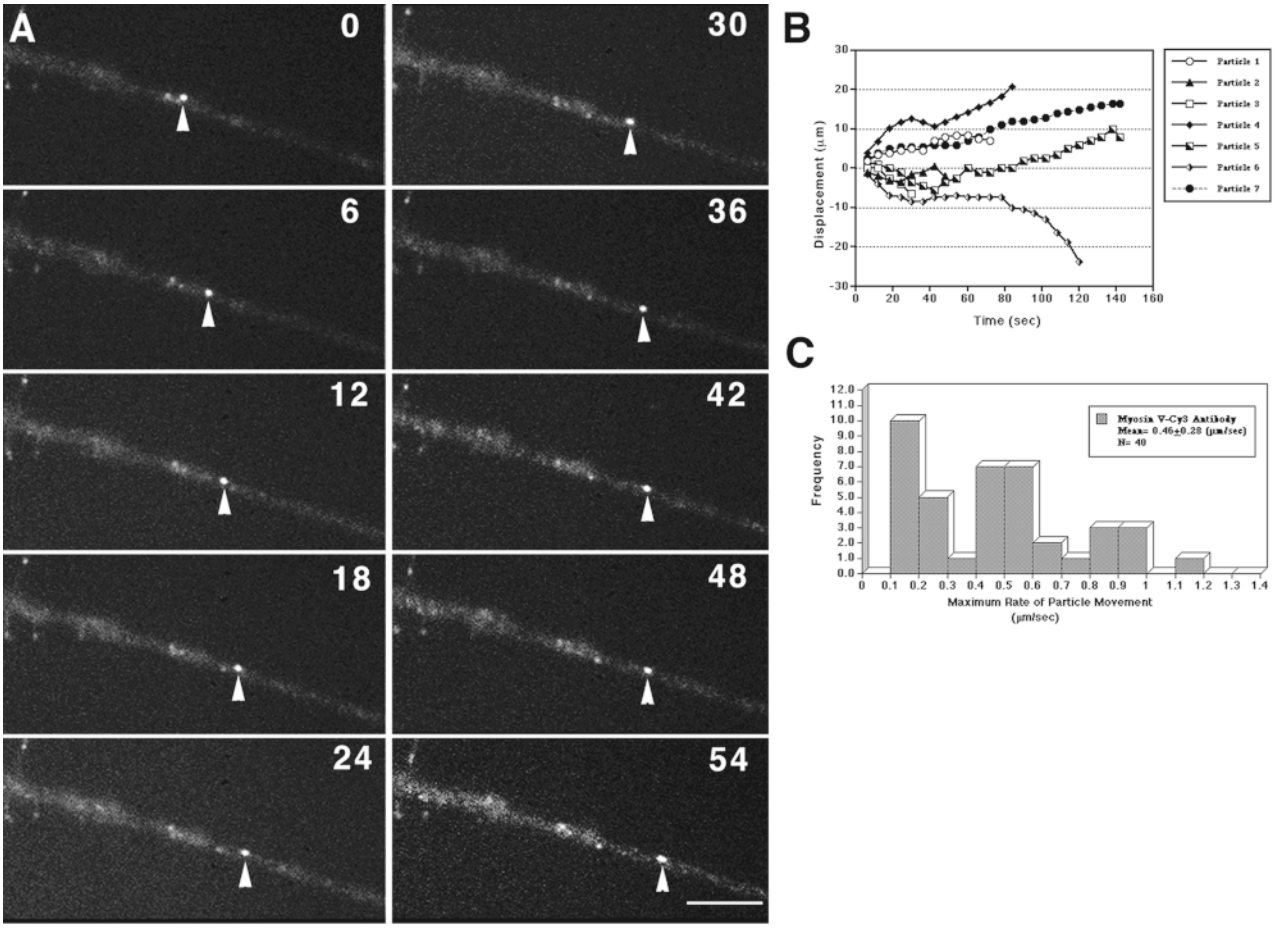

Figure 2. (A) Time-lapse sequence showing a myosin Va-Cy3 antibody-labeled spot (particle) (arrowhead) making anterograde movements along a rat SCG neurite. Only the small relatively dim spots (visible using a 100× 1.4 NA lens) such as the one shown in this sequence, exhibited rapid movements. Large bright spots seen in cell bodies and proximal neurite segments of neurons injected with larger amounts of antibody never made rapid movements. The interval between images is 6 s. (B) The displacement of individual myosin Va-Cy3 antibody spots (particles) at sequential time points is shown. Positive values indicate movement away from the cell body, negative values indicate movement towards the cell body. Movement is saltatory; pauses and direction reversal can occur for varying periods of time. All examples are from rat SCG neurons. (C) The maximum rates of particle movements from untreated neurons (rat, $n = 27$; mouse, $n = 13$) show a wide distribution. Bar, 6.4 μm.

for analysis, there was an apparent overall bias toward anterograde movement (69%). To determine whether our selection process influenced this result, the direction was scored in three 6-min time-lapse sequences from different cells for every moving spot ($n = 53$). An anterograde bias (62%) was still detected. An anterograde bias is consistent with previous reports on axonally transported vesicles in cultured neurons (Morris and Hollenbeck, 1995; Nakata et al., 1998). However, chi-square analysis using the assumption that transport was equal in both directions (null hypothesis) indicated that the apparent bias was not statistically significant ($P > 0.2$). The maximum rates of movement achieved by small spots were widely distributed (Fig. 2 C). Because we could not make recordings of spot movement with delays between exposures <5 s, it is not possible to be certain of the reason for the variation in maximum rate. Either the spots achieve highly variable maximum rates or movements between time-lapse intervals are sometimes interrupted by short pauses at irregular intervals. The time-lapse data is clearly influenced by pauses and transient direction reversals, since the average rate of particle movement was considerably less (0.18 ± 0.09 μm/s, $n = 24$) than the mean maximum rate (0.46 ± 0.28 μm/s, $n = 40$).

To determine whether the movements of the microinjected myosin Va-Cy3–labeled antibodies were characteristic of a set of structures that are uniquely associated with myosin Va, some rat SCG neurons were microinjected with an affinity purified myosin 1α-Cy3 antiserum (Lewis and Bridgman, 1996). The pattern of fluorescent spots that formed was identical to that observed in fixed cells stained with the myosin 1α antiserum. Fluorescent spots were both stationary and moving. The movement was bi-directional. The mean maximum rate of particle movements from myosin 1α labeled structures was significantly slower (0.09 ± 0.08 μm/s, $n = 12$; *t* test, $P < 0.001$) than those la-

beled with antibodies to myosin Va. The slower rate of movement of the myosin 1α-Cy3 fluorescent spots suggest that the two different antibodies are reacting specifically with different populations of transported structures.

Partial Colocalization of Myosin Va-Cy3–labeled Spots with a Marker for Synaptic Vesicles

To determine the identity of the myosin Va-Cy3–labeled spots in microinjected cells, some SCG cultures (six) were fixed, permeabilized, and labeled with mAb antibodies to the synaptic vesicle proteins, SV2 and synaptophysin (Evans et al., 1998). SV2 label showed partial colocalization (49%) with the small spots of myosin Va-Cy3 antibody (n = 129) in neurites (Fig. 3 A). This partial colocalization was apparent in cell bodies, varicosities, and enlarged neurite terminations (possible presynaptic terminals), but was difficult to quantitate because of the increased thickness. The partial colocalization may result from the limited amount of myosin Va-Cy3 antibody microinjected. Consistent with this possibility, neurons injected with higher concentrations of antibody that showed large bright spots of antimyosin Va-Cy3 antibody also showed large bright spots of SV2 label (Fig. 3 B). Superimposition of images showed that all of the large bright spots in neurites colocalized and smaller SV2 spots were no longer detectable. This suggests that the higher concentration of the myosin Va antibody coaggregated most, if not all, of the available SV2.

SV2 and synaptophysin have been reported to be axonally transported in different organelle compartments (Okada et al., 1995; Yonekawa et al., 1998). To determine whether both of these organelle compartments are transported in association with myosin Va, a mAb to synaptophysin was also used for labeling. In contrast to the results with the SV2 labeling, immunofluorescence labeling of injected neurons with a monoclonal antibody to synaptophysin produced only very limited colocalization between the two labels. In neurites, the colocalization was minimal (≤4%). Neurons with large bright spots of myosin Va-Cy3 label occasionally showed corresponding bright spots of synaptophysin label. However, these spots were usually smaller than the myosin Va-Cy3 spots. In addition, many small spots of synaptophysin label still filled the cell body, indicating that most of the synaptophysin was not coaggregated by the microinjected antibody. In cultures that were 3 d or older, enlarged terminations formed in close opposition with other neurons (possible synaptic contacts). In neurons injected with low concentrations of antibody, bright staining with both synaptophysin and myosin Va-Cy3 labels was observed within these structures, but it was difficult to determine the degree of overlap because of their thickness.

Microinjected Myosin Va-Cy3 Antibodies Label Organelles

The colocalization of the microinjected myosin Va-Cy3– and SV2-labeled antibodies provides support for the vesicle association of myosin Va. To test this assumption, two types of ultrastructural analysis were used. First, the microinjected myosin Va-Cy3–labeled antiserum was photoconverted to an electron-dense reaction product, visualized by thin section EM. This method avoids the permeabilization of the injected cells. Second, a gold-conjugated secondary antibody was applied to microinjected neurons that had been permeabilized with saponin.

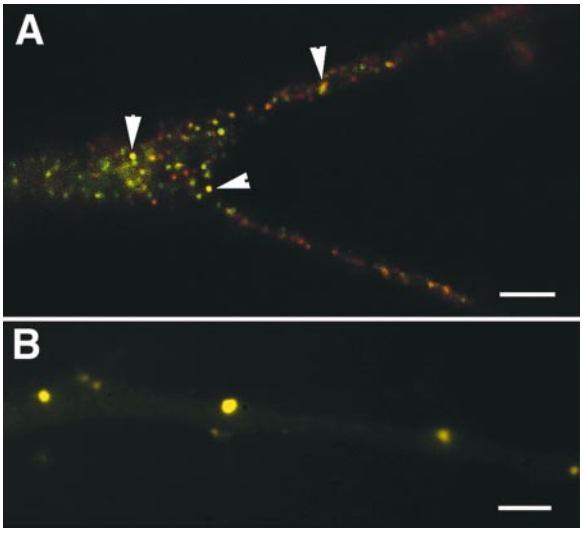

Figure 3. The microinjected myosin Va-Cy3 antibody partially colocalizes with anti–SV2 labeling. (A) From a rat SCG neuron microinjected with a low concentration of the conjugated antiserum. Red is the myosin Va-Cy3 antibody and green is the monoclonal anti–SV2 staining. Yellow indicates that many of the spots (arrowheads) correspond. (B) From a rat cell that was injected with a higher concentration of the myosin Va-Cy3 antibody and then fixed and stained as in A. The large spots are yellow, indicating staining for both myosin Va and SV2 in all visible spots. Experiments done with an unconjugated myosin Va antibody also produced large spots that stained with the SV2 monoclonal antibody (not shown). Bars: (A) 2.5 μm; (B) 3.6 μm.

In photoconversion experiments, neurons microinjected with low concentrations of myosin Va-Cy3 antibody that were clearly intact after fixation (noninjured or degenerating as indicated by phase contrast and fluorescence microscopy) showed dark reaction product surrounding individual vesicle profiles in neurites (Fig. 4, A and B). Neurons injected with higher concentrations of the myosin Va-Cy3 antiserum that showed the large bright spots by fluorescence microscopy also contained larger discrete areas of dark granular reaction product in cell bodies and proximal neurites (Fig. 4 C). These areas were always associated with multiple organelle profiles, suggesting that the antibody aggregated vesicles through its cross-linking ability. Controls (noninjected cells subjected to irradiation) showed no reaction product.

In one experiment, a microinjected cell showing only the small spots of myosin Va-Cy3 fluorescence was fixed, permeabilized, and then incubated with a secondary antibody conjugated to 6 nm colloidal gold. Thin sections from this cell showed discrete labeling of individual structures that resembled organelle profiles (Fig. 4 D). These results indicate that the rapidly moving spots in neurites of cells microinjected with the myosin Va-Cy3 antiserum are likely to be individual vesicles.

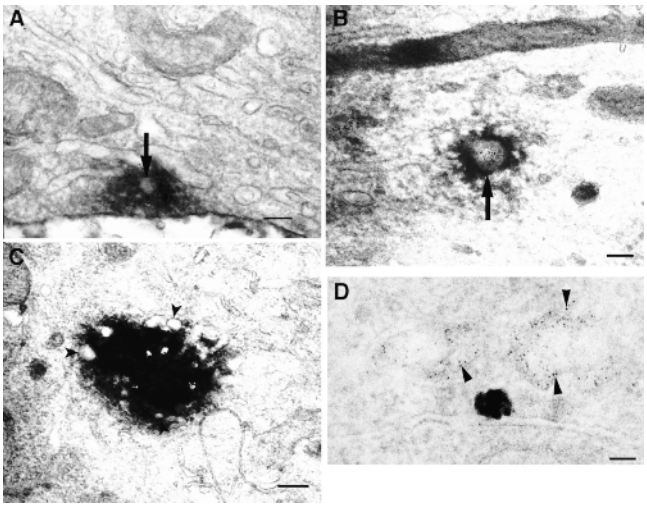

Figure 4. Photoconversion of the microinjected myosin Va-Cy3–labeled antibody produces dark reaction product spots that are associated with organelles. (A and B) Two examples showing organelles in neurites that extended from different identified rat neuronal cell bodies injected with low concentrations of the antiserum. In both cases, single vesicle profiles are surrounded by dark reaction product (arrows). (B) A thin section from a photoconverted rat neuronal cell body that was injected with a high concentration of the myosin Va-Cy3 antiserum. This cell body contained large bright fluorescent spots before photoconversion. Membrane-bound organelles (arrowheads) surround the dark reaction product. The light spots within the dark area probably represent vesicle profiles. (D) A thin section from a rat neuronal cell body microinjected with a low concentration of antibody. This cell was permeabilized and then incubated with 6 nm gold-conjugated anti–rabbit antibody instead of photoconversion. The small gold particles label two irregular shaped membrane profiles (part of the membrane surface is within the section thickness). Bars: (A–C) 180 nm; (D) 70 nm.

Colocalization of a GFP–Myosin Va Tail Fusion Protein Fluorescence with Antibody Staining for Myosin Va and SV2

A different method of marking myosin Va–associated organelles was necessary to: (a) control for the possible effects of surface antibody binding on myosin Va function, and (b) allow labeling of myosin Va–associated structures in *dilute-lethal* neurons. There is evidence that the globular tail portion of the myosin Va protein is responsible for its putative interaction with organelle surfaces (Cheney et al., 1993). Expression of a GFP–myosin Va construct containing this domain would be expected to produce a fusion protein capable of binding to organelles. In melanocytes, cultured cells and yeast expression of similar constructs have been shown to target the tail truncate to the full-length myosin V's normal location (Bizario et al., 1998; Wu et al., 1998; Reck-Peterson et al., 1999). At appropriate expression levels, this would provide a marker for individual organelles that normally associate with native myosin Va. To determine if a rat GFP–myosin Va tail construct could act as an appropriate marker, we expressed it (designated as GFP–myosin Va-t) in cultured SCG neurons. We then used immunofluorescence with a myosin Va antibody (Dil-2, gift of John Hammer) that was treated so that it lacked reaction with the expressed fusion protein to determine if it was correctly targeted in mouse neurons. Most heterozygous cell bodies appeared bright and fluorescence could be detected at low magnification in all neurites emerging from the cell body. At higher magnification, the fluorescence consisted mainly of bright spots of varying size and intensity. In cell bodies, bright irregular shaped spots were frequently seen in the perinuclear region and near the plasma membrane. Large bright spots were also seen in proximal portions of some neurites, but most neurites contained only small spots. Terminal varicosities in older cultures (>2 d) contained many small dim spots and an occasional bright spot of fluorescence. Nearly complete overlap in the distribution of GFP–myosin Va-t and myosin Va immunofluorescence label was observed in thin neurites (Fig. 5, A and B). Similar overlap was seen in cell bodies, growth cones, or terminal, but the increased thickness made it more difficult to determine the precision of the colocalization. The exception was very bright large GFP spots (possibly vacuoles) located in a few cell bodies that increased in size and number with time in culture. Similar large very bright spots were seen in most nonneuronal cells. The large very bright spots showed weak or no colocalization with myosin Va antibody staining (not shown). We assume that the very bright spots in these cell bodies (and nonneuronal cells) represent sequestered and/or degraded GFP–myosin Va-t fusion protein. Cells showing such large bright spots were not used for analysis of spot movement or cell body brightness. *Dilute-lethal* neurons showed a similar distribution of the GFP–myosin Va-t. However, no specific DIL-2 antibody staining was seen in the cells expressing GFP–myosin Va-t, indicating that the antibody did not recognize the expressed myosin Va tail fusion protein (Fig. 5, C and D).

Colocalization of the GFP-myosin Va-t small spots of fluorescence with SV2 immunofluorescence were also observed in cells fixed and then stained with a monoclonal antibody to SV2 (Fig. 5, E and F). Although we did not quantitate the degree of colocalization, it resembled that seen with the microinjected myosin Va-Cy3 antibody.

Dynamics of a GFP-Myosin Va-t in Cultured SCG Neurons from Normal Rats or Heterozygous Mice and Dilute-Lethal Mice

To compare the dynamics of myosin Va–associated organelles in normal and *dilute-lethal* neurons, we used time-lapse recording to obtain quantitative data on their movements in neurons transfected with myosin Va-t. Unexpectedly, expression of the GFP-myosin Va-t construct in neurons cultured from *dilute-lethal* mice resulted in bright spots with similar characteristics to those observed in neurons from rats and heterozygous mice (Fig. 6). Small bright fluorescent spots were distributed along the entire length of both *dilute-lethal* and control neurites. No detectable accumulation of bright spots was observed in cell bodies of *dilute-lethal* neurons. Consistent with this observation, the peak brightness of neuronal cell bodies from heterozygous or *dilute-lethal* mice showed no significant difference ($P > 0.2$; heterozygous = 9,982 ± 3,220 iu, $n = 4$, *dilute-lethal* = 7,765 ± 2,424 iu, $n = 5$). Surprisingly, ~10% of the spots

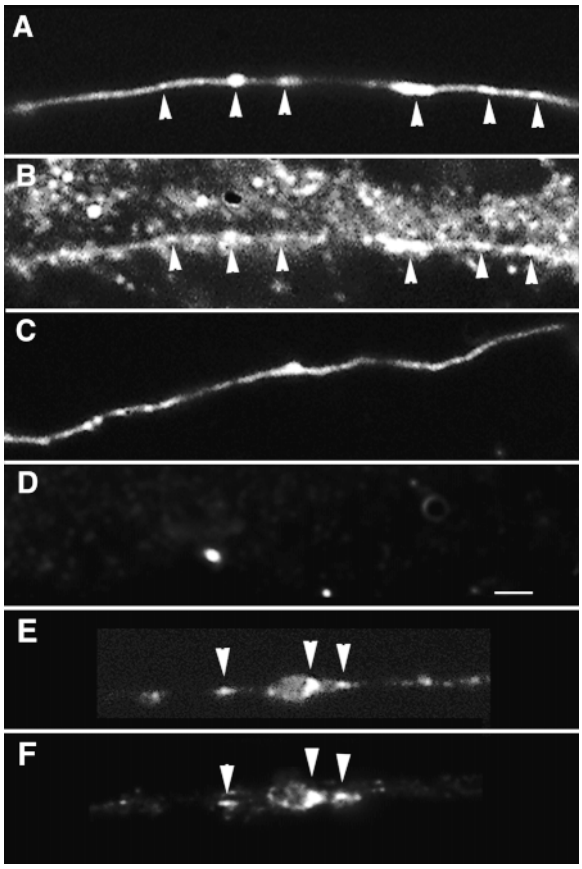

Figure 5. GFP-myosin Va-t fluorescence is correctly targeted in neurons as indicated by colocalization with immunofluorescence staining for myosin Va or SV2. The DIL-2 antibody to myosin Va used for staining was made to amino acids 910–1106 of the myosin Va heavy chain (Wu et al., 1997). This overlapped by two amino acids with the sequence used for the GFP-myosin Va-t fusion protein. To remove a cross-reacting epitope resulting from this overlap, the antiserum was preincubated with a purified GST-myosin Va-t fusion protein coupled to agarose beads. The beads were pelleted by centrifugation and the supernatant used for immunofluorescence staining. (A) GFP-myosin Va-t fluorescence in a neurite from a heterozygous mouse. Arrowheads indicate bright spots of staining along the length of the neurite. (B) Immunofluorescence image of the same area as in A using the preabsorbed DIL-2 antibody. Bright spots of fluorescence (arrowheads) in the neurite correspond with the bright spots seen in A. The neurite lies along the surface of nonneuronal cells that also show bright spots of antibody stain. (C) GFP-myosin Va-t fluorescence in a neurite from a *dilute-lethal* mouse. (D) Immunofluorescence image of the same area as in C using the preabsorbed DIL-2 antibody. The fluorescence does not colocalize, indicating that the preabsorbed antibody does not cross-react with the GFP-myosin Va-t fusion protein. The few bright spots observed are nonspecific staining. (E) GFP-myosin Va-t fluorescence in a neurite from a heterozygous mouse. (F) Immunofluorescence image of the same area as in E using a mAb to SV2. The brightest spots in the two images show colocalization (arrowheads). Bar, 1.5 μm.

in any one sequence recorded from neurites of *dilute-lethal* neurons were undergoing rapid movements. Since myosin Va cannot be the motor in *dilute-lethal* neurons, other motor proteins must be responsible for the movement. Similarly, recordings from transfected SCG neurons from rat embryos or heterozygous mice revealed that ~10% of the fluorescent spots in neurites were undergoing movement (Fig. 6). To determine whether small spots that remained stationary in neurites during an entire sequence of recording might represent a different population than moving spots, we compared their peak brightness. Consistent with this idea, the stationary spots gave a brighter mean value (2,865 ± 1,089 iu, $n = 21$) than moving spots (1,065 ± 426 iu, $n = 14$), and the difference was significant (*t* test, $P < 0.001$). Similar to the microinjected myosin Va-Cy3 antiserum, sometimes spots that were stationary at the start of recording began to move and motile spots stopped moving (and were therefore categorized as moving spots). Moving spots also showed short pauses and direction reversals characteristic of saltatory movement (Fig. 6 C). Movement was bi-directional and was biased toward anterograde movement. In *dilute-lethal* neurons, 88% of the spots analyzed for speed (21/24) moved in the anterograde direction. We also scored the direction of movement of all spots in eight sequences. Again, the movement was predominantly in the anterograde direction (26/30 or 87%). In contrast, in the rat or heterozygous neurons, only 64% percent of the spots selected for quantitative analysis made anterograde movements. In five 6-min time-lapse sequences, the directions of all moving particles were scored. 68% (23/34) made anterograde movements. While chi-square analysis indicated that the apparent anterograde bias observed in neurites from rat or heterozygous mice was not statistically significant, the anterograde bias observed in *dilute-lethal* neurites was significant ($P < 0.01$).

There was no detectable difference in maximum or average rates observed in SCG neurons from rats compared with heterozygous mice and so the results have been pooled (Fig. 6 D). The maximum rate was significantly greater (*t* test, $P < 0.02$) than that obtained with the microinjected myosin Va-Cy3 antibody. However, the average transport rates were the same (myosin Va-Cy3 antibody = 0.18 ± 0.09, $n = 40$ vs. GFP-myosin Va-t = 0.15 ± 0.07 μm/s, $n = 23$). Comparison of the maximum rates of particle movements in cells derived from rats and heterozygous mice to those in cells from *dilute-lethal* mice indicated that the latter were significantly faster (Fig. 6, D and F, *t* test, $P = 0.01$). Thus, myosin Va activity may dampen the speed of organelle transport similar to that observed in melanocytes (Wu et al., 1998; see also Morris and Hollenbeck, 1995). However, the average rates were not significantly different (0.15 ± 0.07 μm/s, $n = 23$ vs. 0.22 ± 0.21 μm/s, $n = 21$, $P > 0.1$), because the pauses and direction reversal have more impact on the average rate than the small difference in maximum rate.

Nocodazole Treatment Alters the Dynamics of Myosin Va–associated Organelles in Cultured SCG Neurons

The above results indicate that motors other than myosin Va must contribute to the movement of myosin Va–associated organelles. The high rates of movement suggest that microtubule motors might be involved. To determine whether microtubules were necessary for the rapid movements of myosin Va–associated organelles, chronic application of nocodazole was used to depolymerize microtu-

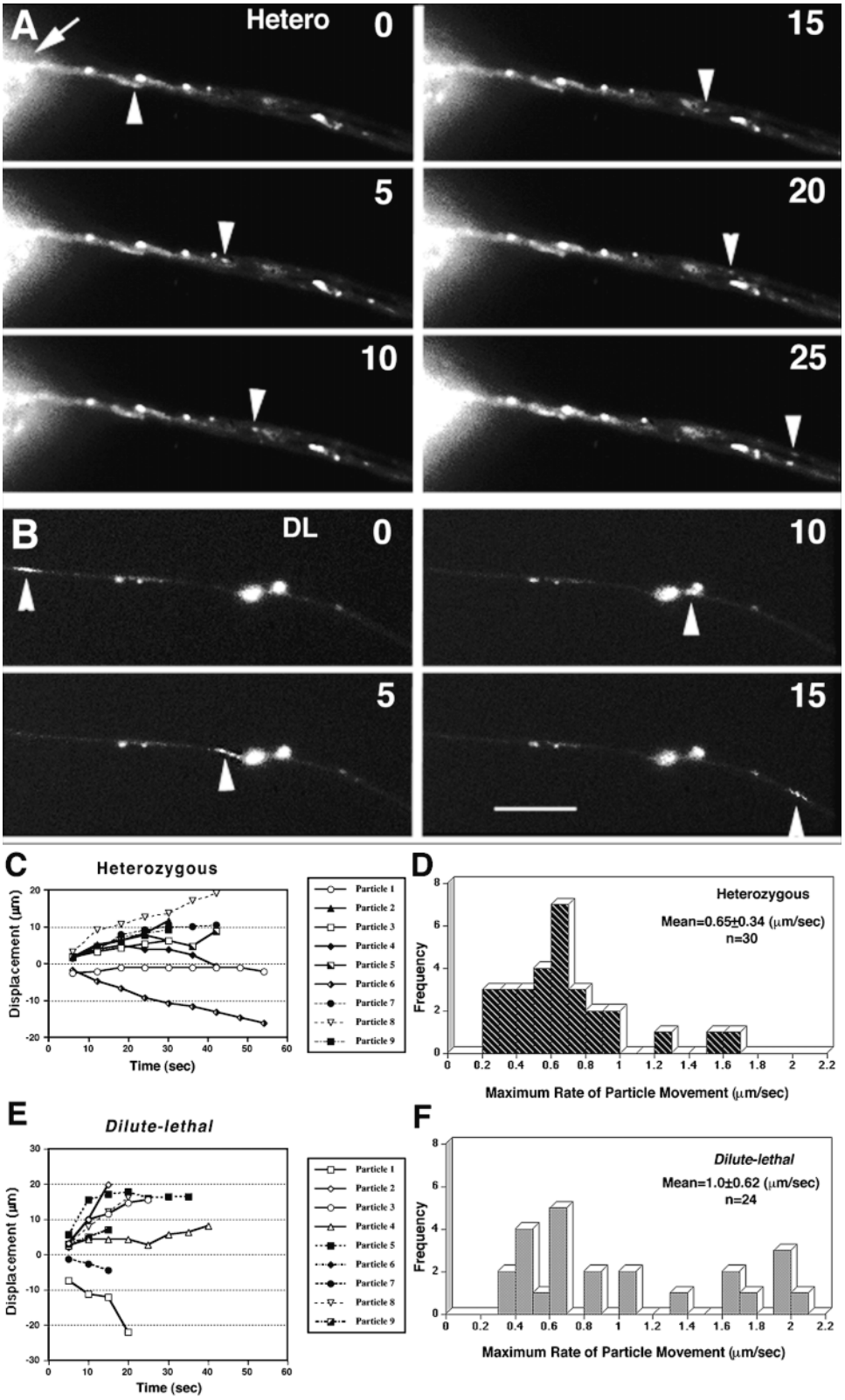

Figure 6. Sequences showing movement of GFP-myosin Va-t in SCG neurons derived from heterozygous (A) and *dilute-lethal* (B) mice. Stationary and moving spots (arrowheads) are observed in axons from both types of mice (5-s intervals are depicted). A portion of the cell body (arrow) is seen in A. The moving spot in B is elongated or a series of connected spots. (C) Displacement over time of individual GFP-myosin Va-t particles in SCG neurons derived from heterozygous mice. Bidirectional movements are observed. (D) The maximum rate of particle movements observed in neurites from heterozygous mice (n = 23) and rats (n = 7). (E) Displacement over time of individual GFP-myosin Va-t in SCG neurons derived from *dilute-lethal* mice. Particles in *dilute-lethal* neurons tended to make larger jumps between time points. (F) The maximum rate of particle movements observed in neurites from *dilute-lethal* mice. The maximum rates achieved for some particles are greater than those observed in neurons from heterozygous mice. Bar, 5.8 μm.

bules. Cells were plated and then grown in the continuous presence of the nocodazole (3.3 μg/ml) for 3–6 d (Morris and Hollenbeck, 1995). Microtubules were completely eliminated from the broad lamellae and short processes produced by the treated neurons under these conditions (Fig. 7). Despite the difference in morphology, nocodazole-treated cells microinjected with myosin Va-Cy3 antibody showed a similar distribution of fluorescent spots to untreated cells (Fig. 7). Fluorescent spot movements were still apparent in time-lapse recordings, but moved at re-

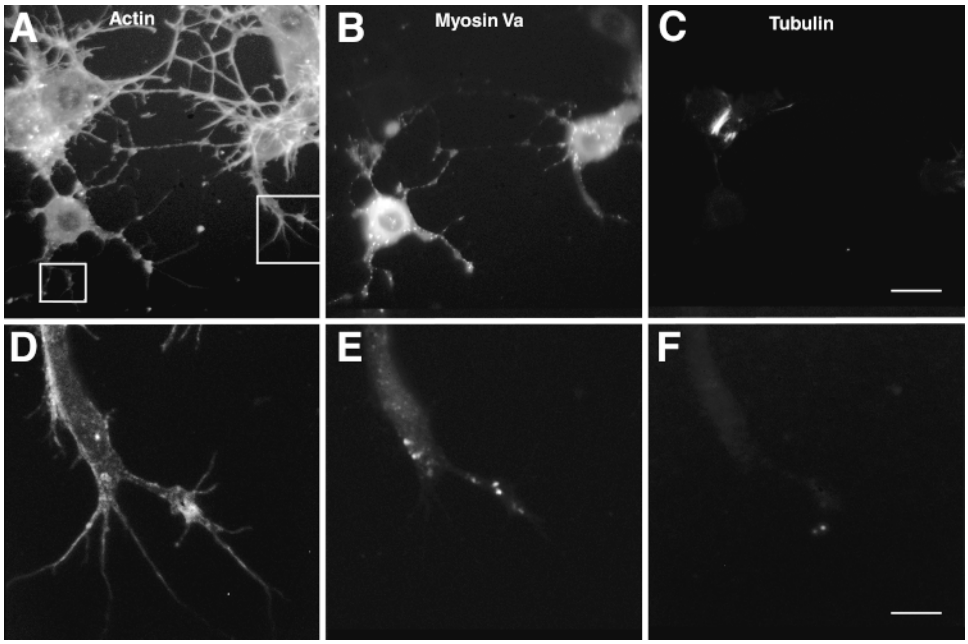

Figure 7. Rat SCG neurons grown for 3 d in nocodazole (3.3 μg/ml), and then microinjected with anti–myosin Va-Cy3 antibody lack microtubules in cell processes. The distribution of actin (A and D), microinjected myosin Va-Cy3 antibody (B and E), and microtubules (C and F) are shown in two cells (B) used for recording movements of myosin Va-Cy3 antibody spots. The boxed regions in A indicate the areas used for recordings. Although some residual microtubule segments can be observed in the perinuclear region of one noninjected cell (C), they are absent from cell processes that extend peripherally in the injected cells (C and F). D and F are high magnifications of a portion of the cell indicated by the boxed region (right side) in A. Bars: (A–C) 21.5 μm; (B–F) 5 μm.

duced rates (Fig. 8, A and E). Fluorescent spots (particles) paused and reversed direction more frequently than in untreated cells (compare Figs. 8 A and 2 B). A sizable and significant decrease (*t* test, $P < 0.001$) occurred in maximum rate (0.1 ± 0.05 μm/s, $n = 12$) in the absence of microtubules (compare Figs. 8 E and 2 C).

Similarly, SCG neurons from embryonic rats or P0 heterozygous mouse pups cultured for 3 d in medium containing nocodazole and then transfected with GFP-myosin Va-t showed fluorescent spots distributed throughout the entire length of their short processes. Time-lapse recordings revealed that small spots in the short neurite-like processes moved at significantly reduced average and maximum rates (*t* test, $P < 0.001$) compared with untreated cells (Fig. 8, B and F). After recordings, cultures were fixed and immunofluorescently stained for actin and microtubules. Identical to cells used for antibody microinjection, short microtubules segments were sometimes observed in the perinuclear region, but most cells lacked microtubules in the broad lamellae and short neurite-like processes used for time-lapse recordings.

In cells from *dilute-lethal* mice that were grown under a modified nocodazole treatment protocol, GFP-myosin Va-t fluorescent spots were absent from the distal portions of processes, but were present at the base and in more proximal portions. Time-lapse recordings indicated that the small fluorescent spots within the processes appeared to make only short back and forth movements. Quantitative analysis indicated that the net displacement of spots during the recordings were extremely small (Fig. 8 C). The calculated rates of movement (maximum $= 0.04 \pm 0.01$ μm/s, average $= 0.005 \pm 0.004$ μm/s, $n = 19$) were significantly less (*t* test, $P < 0.001$) than the maximum and average rates of movements seen in heterozygous cells treated with nocodazole. This suggests that the small back and forth movements that were observed were not directed, but are likely to be Brownian-like. The very small rate of displacement was the same as the slow movement of large bright spots observed in cells microinjected with high concentrations of myosin Va-Cy3 antibody. This movement may result from other non–myosin Va-dependent mechanisms. Similar slow movements have been reported in *dilute-lethal* melanocytes (Wu et al., 1998).

Dilute-lethal cultures used for recordings were fixed and labeled with rhodamine phalloidin and a monoclonal antibody to tubulin to reveal the distribution of F-actin and microtubules. Similar to cells plated directly in nocodazole, microtubules were sometimes present in the perinuclear region, but were absent from the lamellae and most short processes that extended from the cell body. Unlike cells plated directly in nocodazole, very small, discontinuous microtubule segments were occasionally observed in the shortened processes, suggesting that some microtubule segments formed in processes before nocodazole exposure were stabilized. However, in the processes of nocodazole-treated cells from *dilute-lethal* mice, we never observed movements of GFP-myosin Va-t that were clearly directed.

Latrunculin Treatment Does Not Significantly Effect Myosin Va–associated Organelle Movement

To determine whether actin-based motors might contribute to the rapid movements of myosin Va–associated organelles, SCG neurons from heterozygous mice were grown for 3 d in medium containing latrunculin A. Neurons had altered morphology (Marsh and Letourneau, 1984), and lacked detectable actin filaments when stained with rhodamine phalloidin (not shown). Neurons expressing GFP-myosin Va-t showed fluorescent spots distributed along the entire length of their processes. Time-lapse recordings revealed the rapid movement of small GFP-myosin Va-t spots in neurites (Fig. 8 D). The maximum rates of movement were significantly greater (*t* test, $P < 0.001$)

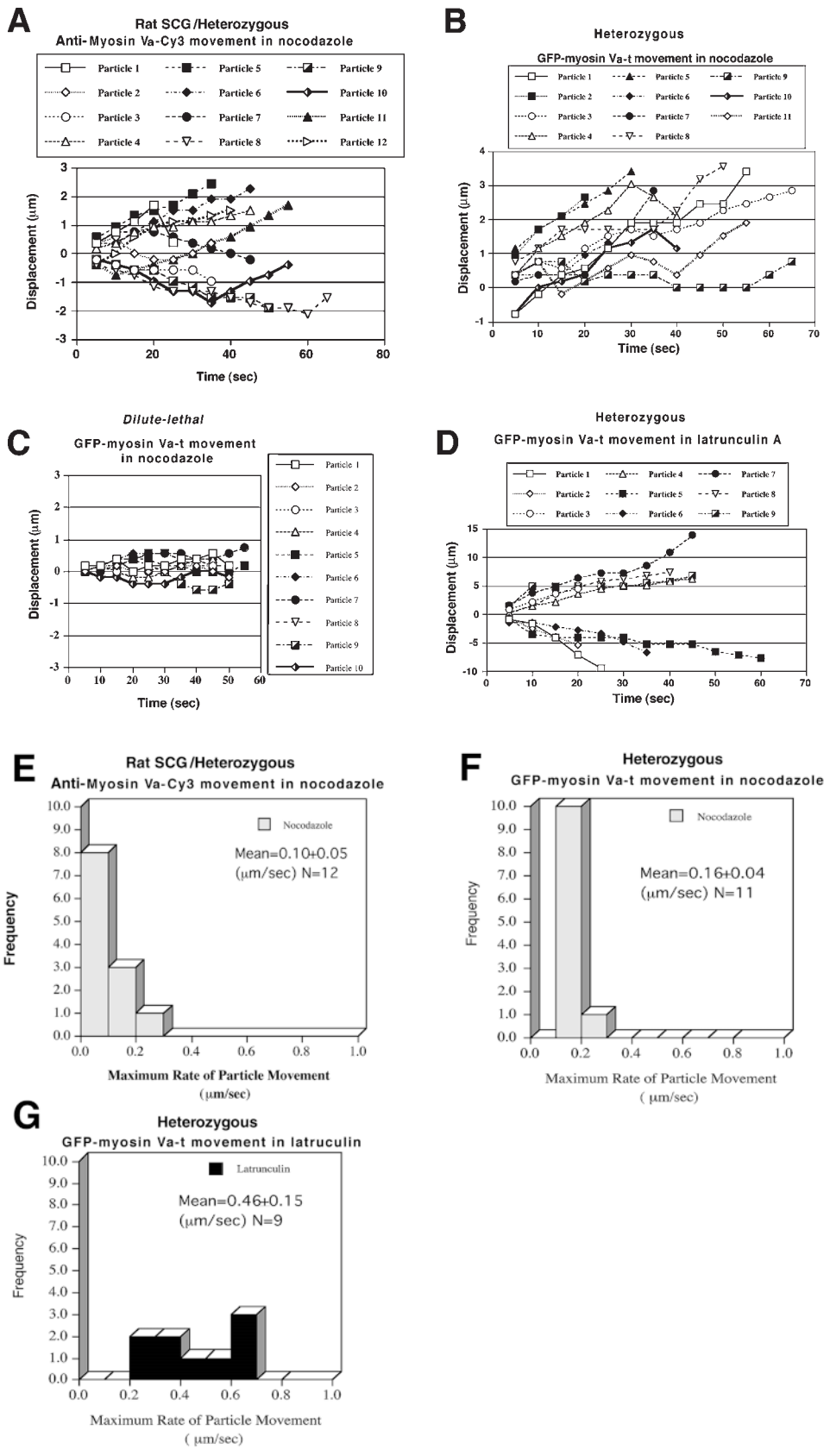

Figure 8. Quantitative analysis of myosin Va (antibody or GFP-myosin Va-t) movements in neurites treated with nocodazole and latrunculin A. (A) The displacement of individual myosin Va-Cy3 antibody spots (particles) along neurites in rat cells grown for 3 d in nocodazole. The displacement between time points is much less than in untreated cells (see Fig. 2). Pauses and direction reversals appear more numerous than in untreated cells. Positive values indicate movement away from the cell body. (B) The displacement of individual GFP-myosin Va-t spots along neurites in SCG neurons from heterozygous mice grown for 3 d in nocodazole. Movement is saltatory; particles pause and temporarily reverse direction, but progress generally in a single direction. (C) The displacement of individual GFP-myosin Va-t spots in neurons from *dilute-lethal* mice grown in nocodazole. The particles oscillate around the zero point. (D) The displacement of individual GFP-myosin Va-t spots along neurites in SCG neurons from heterozygous mice grown for 3 d in latrunculin. Movement is greater between time points, is bi-directional, and shows fewer pauses and direction reversals than in nocodazole. (E) The maximum rate of myosin Va-Cy3 antibody spot movement in cells grown for 3 d in nocodazole. The mean maximum rate of movement is significantly slower (*t* test; $P < 0.001$) than in untreated cells (see Fig. 2). (F) The maximum rates of GFP-myosin Va-t spot movement in SCG neurons from heterozygous mice grown for 3 d in nocodazole. The mean maximum rate shows a large decrease compared with maximum rates of movement in untreated or latrunculin-treated neurons. (G) The maximum rates of GFP-myosin Va-t spot movement in SCG neurons grown for 3 d in latrunculin. The mean of the maximum rates of GFP-myosin Va-t movements are significantly greater (*t* test; $P < 0.001$) in latrunculin compared with nocodazole.

than those observed in nocodazole-treated cells (Fig. 8 G). Although the maximum rate of spot movement was slightly less than the maximum rate observed in untreated cells, the difference was not significant (*t* test, $P = 0.1$). This indicates that actin-based motors are not necessary for rapid movements in axons

Comparison of SV2 and Synaptic Vesicle Distribution in Neurons from Heterozygous and Dilute-Lethal Mice

If the capture model for melanosome accumulation in peripheral dendrites of melanocytes (Wu et al., 1998) holds for myosin Va–associated organelle distribution in neurons from *dilute-lethal* mice, then one would predict: (a) a concentration of myosin Va–associated organelles within cell bodies of neurons, and (b) a depletion of the same organelles from their peripheral target.

We had not observed accumulation of GFP-myosin Va-t label in cell bodies of *dilute-lethal* neurons. However, because the observations were done at relatively short times (<20 h) after the beginning of the GFP-myosin Va-t expression, it is possible that accumulation would only be detected with increased time.

To address this possibility, the distributions of anti–SV2 label in 3-d-old dissociated cultures of SCG neurons from heterozygous and *dilute-lethal* mice were compared. Because SV2 shows a high degree of colocalization with bright spots of myosin Va, it should provide a good independent marker of myosin Va–associated organelles. The peak brightness of SV2 label in cell bodies of *dilute-lethal* neurons was slightly greater than those from heterozygous controls (*dilute-lethal* = 778 ± 45 iu, $n = 4$ vs. heterozygous = 639 ± 48 iu, $n = 8$), but the difference was not significant ($P > 0.1$). This indicates that SV2 does not accumulate in cell bodies of *dilute-lethal* neurons, consistent with the observation that transport of myosin Va–associated organelles is biased towards anterograde movement.

The brightness of SV2 label was also compared in regions that showed the brightest SV2 label in neurites: varicosities, branch points, and axon terminations. The comparison was done under two different culture conditions: in 3-d-old low-density dissociated cell culture (cells were not contacting each other), and in explants grown for 5 d. In the low-density dissociated cultures, varicosities, branch points, and terminations of *dilute-lethal* neurons showed a significant increase ($P < 0.001$) in peak brightness (*dilute-lethal* = 1,068 ± 220 iu, $n = 11$ vs. heterozygous = 678 ± 89 iu, $n = 14$), indicating that SV2 does accumulate peripherally within these regions.

The regions showing accumulation of SV2 label also colabeled with a monoclonal antibody to tyrosinated tubulin (Fig. 9). Since tyrosinated tubulin is associated with dynamic plus ends of microtubules, it suggests that these regions contain dynamic microtubule ends. The degree of colocalization was 100%. In other words, the presence of bright SV2 label could predict the occurrence of bright tyrosinated tubulin label and vice versa. To insure that the low density of cells were not affecting the accumulation of SV2, the peak brightness of SV2 label was also compared in neurites of 5-d-old explant cultures. Under these condi-

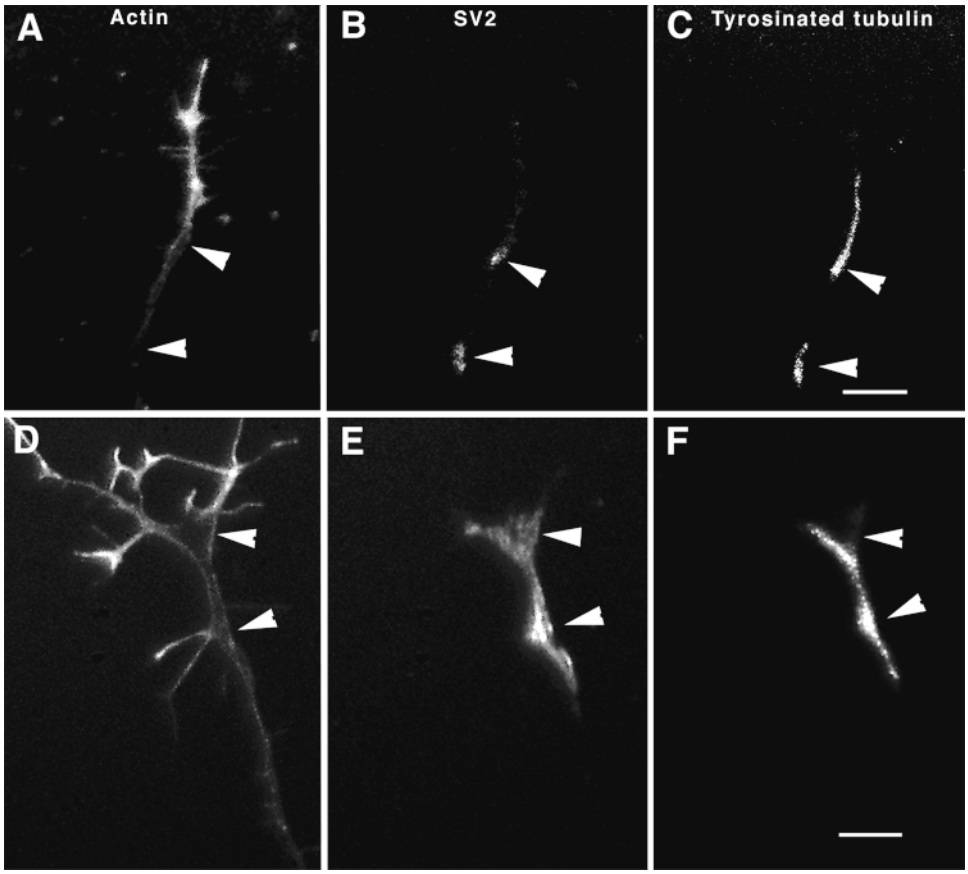

Figure 9. SV2 accumulates in axon terminations of heterozygous and *dilute-lethal* neurons that are rich in tyrosinated tubulin. (A) The actin distribution is depicted in the terminal portion of an axon from a SCG neuron grown from a heterozygous mouse. (B) Wide areas of the axon (arrowheads in A) show increased staining for SV2 (arrowheads). (C) The areas of SV2 accumulation also correspond to the brightest areas (arrowheads) of tyrosinated tubulin staining. (D) The actin distribution is shown for a terminal portion of a SCG neurite grown from a *dilute-lethal* mouse. (E) Wide areas of axons (arrowheads in D) show increased bright staining for SV2 (arrowheads). (F) The areas of SV2 accumulation seen in E correspond to bright areas of tyrosinated tubulin staining (arrowheads). Bars, 6 μm.

tions, neurites grow out radially from explants and do not form synapses (outside the body of the explant). *Dilute-lethal* neurons showed significant increases ($P < 0.001$) in the peak brightness of staining in varicosities, (*dilute-lethal* = 6,378 ± 1,289 iu, $n = 14$ vs. heterozygous = 4,155 ± 400 iu, $n = 12$).

Second, the distribution of anti–SV2 antibody label was compared on cryostat sections taken from the cerebellum of either heterozygous or *dilute-lethal* mice. We compared the peak intensity of label in bright puncta in three regions of individual sections: the granule cell layer, the region surrounding Purkinje cell bodies, and the outer portion of the molecular layer. The granule cell layer of the heterozygous sample had a significantly ($P = 0.05$) brighter staining than the *dilute-lethal* sample (heterozygous = 2,905 ± 423, $n = 13$ vs. *dilute-lethal* = 2,538 ± 367, $n = 10$). In contrast, the portion of the molecular layer immediately adjacent to Purkinje cells had significantly ($P < 0.001$) brighter staining in the *dilute-lethal* sample (*dilute-lethal* = 3,342 ± 197, $n = 10$ vs. heterozygous = 2,171 ± 367, $n = 8$). Similarly, the outer portion of the molecular layer had significantly ($P < 0.001$) brighter staining in the *dilute-lethal* sample (*dilute-lethal* = 2,820 ± 536, $n = 42$ vs. heterozygous = 1,974 ± 381, $n = 30$). This suggests that SV2 accumulates to abnormal levels in *dilute-lethal* granule cell axons and presynaptic terminals, similar to the peripheral accumulation in cultured SCG neurons.

Third, the terminal area and density of synaptic vesicles in synapses from heterozygous and *dilute-lethal* mouse littermates were compared in two different presynaptic terminals. The presynaptic terminals of P12 Purkinje cells did not show significant differences ($P > 0.5$) in terminal cross-sectional area (heterozygous area = 1.1 ± 0.24 μm^2, $n = 6$, *dilute-lethal* area = 1.3 ± 0.67 μm^2, $n = 5$) or synaptic vesicle density (heterozygous = 259 ± 89 vesicles/μm^2, *dilute-lethal* = 310 ± 114 vesicles/μm^2). In contrast, the presynaptic terminals of granule cells appeared to have a much larger average terminal cross-sectional area in *dilute-lethal* mice at all ages that were inspected (P10, P12, P14, P15, P18) (Fig. 10). At P18, the difference was more than fivefold (heterozygous area = 0.76 ± 0.36 μm^2, $n = 21$ vs. *dilute-lethal* area = 4.36 ± 3.6 μm^2, $n = 12$, difference was significant, $P < 0.001$). Synaptic vesicle density was somewhat lower in these enlarged *dilute-lethal* terminals (P18 heterozygous = 25 ± 8 vesicle/μm^2, vs. P18 *dilute-lethal* = 18 ± 12 vesicles/μm^2, $P = 0.05$). At P10 the difference in presynaptic terminal area was not as great (heterozygous area = 0.41 ± 0.26 μm^2, $n = 37$ vs. *dilute-lethal* area = 0.96 ± 0.61 μm^2, $n = 22$), but the difference was still significant ($P < 0.001$). P10 is before the onset of seizures in *dilute-lethal* mice (our unpublished observations), indicating that the increase in presynaptic terminal area is not a secondary effect of the seizures. The greater area indicates that the presynaptic terminal volume of granule cells will be increased in *dilute-lethal* mice. Because of the increased volume, the total number of synaptic vesicles in these terminals will be greater.

Finally, the amounts of SV2 label in granule cell presynaptic terminals *of dilute-lethal* and heterozygous mice were compared using immunoelectron microscopy. Presynaptic terminals of labeled P15 *dilute-lethal* granule cells had a significantly greater number of synaptic vesicles per terminal profile compared with heterozygous littermates as a result of the increased terminal area (Table I). However, the number of anti–SV2-labeled synaptic vesicles (and gold particles) per terminal profile were the same (Fig. 10 and Table II). In contrast, *dilute-lethal* presynaptic terminals had slightly more than twice as many large vesicles (>80-nm diameter) per terminal profile that were labeled with the anti–SV2 antibody. In addition, *dilute-lethal* mice had more anti–SV2 label of large vesicles in parallel fibers away from synaptic sites. This suggests that the increased SV2 staining in the molecular layer of the *dilute-lethal* cerebellum observed by fluorescence microscopy is at least partially a result of the increased accumulation of large SV2 positive vesicles in or near presynaptic terminals.

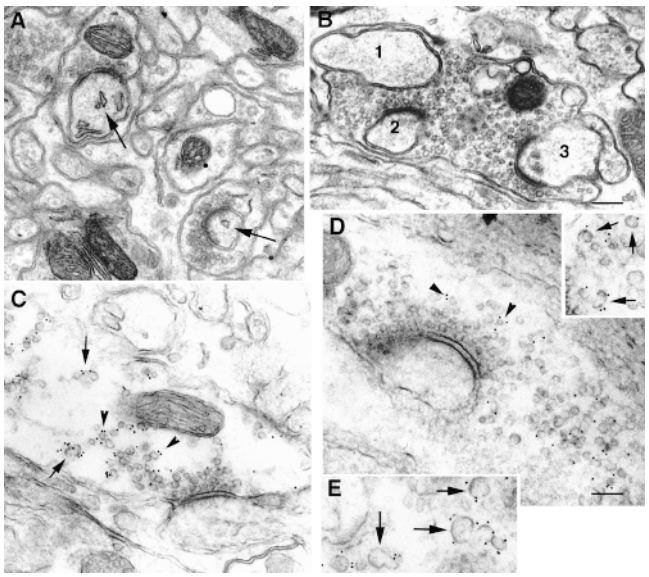

Figure 10. (A) Cross-sectional synaptic profiles of parallel fiber boutons and Purkinje cell dendritic spines from the molecular layer of a P18 heterozygous mouse. Parallel fiber boutons are small and relatively uniform in size. Each bouton contacts a single spine. Purkinje cell spines contain smooth endoplasmic reticulum (arrowheads). (B) Cross-sectional profile of a single large parallel fiber bouton making contact with three (1, 2, and 3) Purkinje cell spines from the molecular layer of a P18 *dilute-lethal* mouse. Spines lack smooth endoplasmic reticulum. (C) The distribution of SV2 antibody label (12 nm colloidal gold) in a parallel fiber bouton from a heterozygous mouse. Many of the synaptic vesicles (arrowheads) are labeled. Some larger vesicles (arrows) also show label in this oblique section. (D) The distribution of SV2 antibody label in a parallel fiber bouton from a *dilute-lethal* mouse. Synaptic vesicles (arrowheads) are labeled. (Inset) From another synaptic terminal showing SV2 antibody label on several larger vesicles (arrows). (E) A nonterminal region of a parallel fiber also shows SV2 antibody labeling of large vesicles in the molecular layer of a *dilute-lethal* mouse. Bars: (A and B) 470 nm; (C–E) 315 nm.

Discussion

Microinjected Myosin Va-Cy3 Antiserum or Expression of GFP-Myosin Va-t Labels Organelles

Two different observations support the conclusion that the microinjected myosin Va-Cy3 antibody labels organelles

Table I. Comparison of Synaptic Vesicle Number and SV2 Immunogold Label in Normal and Dilute-Lethal Parallel Fiber Boutons

Genotype	No. of synaptic vesicles per terminal profile	No. of synaptic vesicles labeled (SV2) per terminal	Percentage synaptic vesicles labeled per terminal	No. of large vesicles labeled (SV2) per terminal	Total No. of vesicle-associated gold particles per terminal	*n*
Heterozygous	46 ± 20*	17 ± 10	37%	0.6 ± 0.9‡	31 ± 19	21
Dilute-lethal	74 ± 29*	15 ± 10	20%	1.5 ± 1.2‡	29 ± 20	17

*Significantly different, *t* test, $P = 0.001$.
‡Significantly different, *t* test, $P < 0.02$.

by binding to their surfaces. First, small spots partially colocalized, and very bright spots showed 100% colocalization, with antibody staining for SV2, an integral membrane protein that is a common marker for synaptic vesicles or their precursors (Feany et al., 1992). Second, ultrastructural observations on photoconverted cells that showed small fluorescent spots represented individual organelles surrounded by DAB reaction product. Large fluorescent spots represented antibody-induced organelle aggregates. In nonphotoconverted cells labeled with colloidal gold particles, individual organelle-like structures were associated with gold label on their surfaces. Thus, the accumulated evidence is most compatible with the external binding and concentration-dependent aggregation of vesicular structures by the microinjected myosin Va-Cy3–conjugated antibodies. The presence of individual labeled organelles within neurites suggests that many of the moving spots observed in time-lapse recordings represent individual vesicles.

The size of the individual labeled organelles found within neurites was highly variable, but in most cases they were much larger (>80 nm) than synaptic vesicles. It has been reported that some synaptic vesicle proteins are axonally transported in pleomorphic vesicles (Nakata et al., 1998). This observation, in combination with the data indicating an almost 50% colocalization with the synaptic vesicle protein SV2, suggests that many of the myosin Va–associated vesicles that move in axons may represent synaptic vesicle precursors. It has also been reported that SV2 is axonally transported in separate organelle compartments from other synaptic vesicle components, including synaptophysin (Okada et al., 1995; Yonekawa et al., 1998). The difference in myosin Va–associated organelle colocalization with SV2 and synaptophysin in neurites is consistent with that observation.

Movement of Myosin Va–associated Organelles in Normal and Dilute-Lethal Axons Occurs at Similar Rates and Is Bidirectional, but in Dilute-Lethal Axons It Is Biased Toward Anterograde Movement

The maximum and average rates of movement of both myosin Va-Cy3 antibody and GFP-myosin Va-t–labeled organelles are similar, suggesting that they act as good markers for myosin Va organelle dynamics. The general characteristics of the movement were also the same. Both were bi-directional and saltatory. Movement of GFP-myosin Va-t–labeled organelles in neurons from *dilute-lethal* animals was also similar to that observed in normal cells, although a bias towards anterograde movement was observed. Furthermore, in untreated cells from both normal and *dilute-lethal* mice, the maximum rates of movement exceed that observed with purified myosin Va–associated vesicles (Evans et al., 1998). Thus, motors other than myosin Va must be responsible for the rapid movements observed. Likely candidates are microtubule-based motors. Consistent with that possibility, the maximum rates of movement are the same as that observed for organelles known to be transported by kinesins (Nakata el al., 1998; Yonokawa et al., 1998).

Rapid Movements of Myosin Va–associated Organelles Are Microtubule Dependent

The maximum rate of myosin Va–associated organelle movement is significantly decreased when normal cells are grown in the presence of nocodazole to prevent microtubule polymerization, indicating that microtubules probably represent the transport tracks responsible for the most rapid movements. Treatment with nocodazole to effectively eliminate microtubules does not stop directed movement. Presumably, F-actin acts as transport tracks under these conditions and the organelles are able to move at reduced rates using myosin motors.

In contrast to normal cells, movements of GFP-myosin Va-t are absent in *dilute-lethal* neurons grown under conditions to eliminate most microtubules. This indicates that myosin Va activity is required for movement of these organelles when microtubules are disrupted. This is the first evidence available to directly support myosin Va–mediated organelle movements in intact neurons. It is consistent with recent observations on melanocytes where myosin Va appears to mediate movement of melanosomes in the absence of microtubules (Wu et al., 1998). Furthermore, it supports the conclusion that individual organelles contain both actin- and microtubule-based motors. While the results only require that both types of motors be present on the same organelle, they are also consistent with the possibility that a single motor complex with dual functions may exist.

Can the Capture Model Explain the Abnormalities Observed in Dilute-Lethal Neurons?

Neurons from *dilute-lethal* mice do not show abnormal accumulations of myosin Va–associated organelles in cell bodies similar to the perinuclear accumulation of melanosomes in melanocytes (Provance et al., 1996; Wei et al., 1997; Wu et al., 1997). The lack of accumulation is likely to be a result of the anterograde bias associated with transport of myosin Va–associated organelles in *dilute-lethal* neurons. The bias could be a result of a change in the balance of retrograde and anterograde microtubule-based motors associated with these organelles. Alternatively, there may be a change in the efficiency of access to microtubule tracks in peripheral regions that contain lower microtubule densities or increased numbers of microtubule

ends. In support of the latter possibility, *dilute-lethal* neurons showed increased accumulations of SV2 label in varicosities, axon branches, and axon terminations. These regions also show staining for tyrosinated tubulin and are near regions that stain for F-actin. Tyrosinated tubulin is associated with portions of microtubules that contain new polymer or, in other words, are close to dynamic plus ends (Kreis, 1987; Schulze et al., 1987). This suggests that myosin Va–associated organelles may become stranded in regions of *dilute-lethal* neurons that have a high concentration of dynamic microtubule plus ends. If this is the case, then it suggests that myosin Va motor activity may facilitate the ability of organelles that have traveled off the ends of microtubules, or are released as a result of depolymerization, to return to these tracks for transport. This is consistent with the reduced percentage of myosin Va–associated organelles undergoing retrograde transport in axons of *dilute-lethal* neurons. Myosin Va may also mediate entry of organelles into the nearby actin-rich regions for short range transport or tethering. The peripheral accumulation of myosin Va–associated organelles in *dilute-lethal* neurons is the opposite of that observed in melanocytes. However, the apparent incompatibility with the capture model presented for melanocytes (Wu et al., 1998) may be primarily a result of differences in the net balance of anterograde and retrograde transport rather than an incompatibility with a myosin Va-dependent tethering.

Dendritic spines of Purkinje cells from P21 mice (a strain obtained from Jackson ImmunoResearch Laboratories, Inc.) have been reported to lack smooth endoplasmic reticulum (Takagashi et al., 1996). We have observed a similar defect in Purkinje cells from *dilute-lethal* (dl-20J/dl-20J) pups (Strobel et al., 1990) at all ages studied (P10–P21). It is not clear if this abnormality fits with a tethering role because the mechanism of spine formation remains controversial (Ziv and Smith, 1996; Fiala et al., 1998).

Dilute-Lethal Mice Have Alterations in a Subset of Presynaptic Terminals

If myosin Va activity is necessary only for local movement or processing of certain organelles in regions devoid of microtubules, then the abnormalities observed in *dilute-lethal* granule cell presynaptic terminals fit with this model. The increased numbers of large SV2-positive vesicles and synaptic vesicles may result from the absence of local transport in *dilute-lethal* axon terminals. Transport of synaptic vesicle to fusion/release sites (active zones) may be defective or loading of vesicles destined for microtubule-based retrograde transport may be abnormal. Either defect could lead to accumulations of vesicles in terminals. However, presynaptic terminals of Purkinje cells did not show any noticeable defects in structure, area, or synaptic vesicle density at P12.

It is unclear why some terminals appear normal and while others are affected. It is especially surprising that Purkinje cell presynaptic terminals do not show defects, since their dendritic spines clearly do (Takagishi et al., 1996; Fig. 10). However, one difference between Purkinje cell presynaptic terminals and those of granule cells is the type of neurotransmitter produced and released. Purkinje cells produce an inhibitory neurotransmitter, while granule cells produce an excitatory neurotransmitter. Possibly there are neuron-specific mechanisms of transport within terminals for different types of synapses. Alternatively, detection of presynaptic structural changes may be activity dependent. Depending on the upstream abnormalities, the output activity (and hence synaptic vesicle turnover) from Purkinje cells may be reduced.

I thank Grady Phillips for expert technical assistance and Drs. John Cooper and John Hammer for comments on the manuscript. Dr. John Hammer generously donated the DIL-2 antibody.

This work was supported by National Institutes of Health grant NS35162 to P.C. Bridgman.

Submitted: 8 April 1999
Revised: 4 August 1999
Accepted: 6 August 1999

References

Bizario, J.C.S., L.C. Rosa, A.A.C. Nascimento, R.E. Larson, and E.M. Espreafico. 1998. Melanosome distribution is affected by expression of chicken myosin-Va constructs in wild type and dilute viral melanoma cells. *Mol. Biol. Cell.* 9:20a. (Abstr.)

Cheney, R.E., M.K. O'Shea, J.E. Heuser, M.V. Coelho, J.S. Wolenski, E.M. Espreafico, P. Forscher, R.E. Larson, and M.S. Mooseker. 1993. Brain myosin-V is a two-headed unconventional myosin with motor activity. *Cell.* 75: 13–23.

Dailey, M.E., and P.C. Bridgman. 1993. Vacuole dynamics in growth cones: correlated EM and video observations. *J. Neurosci.* 13:3375–3393.

Espreafico, E.M., R.E. Cheney, M. Matteoli, A.A. Nascimento, P.V. De Camilli, R.E. Larson, and M.S. Mooseker. 1992. Primary structure and localization of chicken brain myosin-V (p190), an unconventional myosin with calmodulin light chains. *J. Cell Biol.* 119:1541–1557.

Evans, L.L., and P.C. Bridgman. 1995. Particles move along actin filament bundles in nerve growth cones. *Proc. Natl. Acad. Sci. USA.* 92:10954–10958.

Evans, L.L., J. Hammer, and P.C. Bridgman. 1997. Subcellular localization of myosin V in nerve growth cones and outgrowth from *dilute-lethal* neurons. *J. Cell Sci.* 110:439–449.

Evans, L.L., A.J. Lee, P.C. Bridgman, and M.S. Mooseker. 1998. Vesicle-associated brain myosin-V can be activated to catalyze actin-based transport. *J. Cell Sci.* 111:2055–2066.

Feany, M.B., S. Lee, R.H. Edwards, and K.M. Buckely. 1992. The synaptic vesicle protein SV2 is a novel type of transmembrane transporter. *Cell.* 70:861–867.

Fiala, J.C., M. Feinberg, V. Popov, and K.M. Harris. 1998. Synaptogenesis via dendritic filopodia in developing hippocampal area CA1. *J. Neurosci.* 18: 8900–8911.

Harris, K.M., and J.K. Stevens. 1989. Dendritic spines of CA1 pyramidal cells in the rat hippocampus: serial electron microscopy with reference to their biophysical characteristics. *J. Neurosci.* 9:2982–2997.

Hirokawa, N. 1993. Axonal transport and the cytoskeleton. *Curr. Opin. Neurobiol.* 3:724–731.

Huang, J.-D., S.T. Brady, B.W. Richards, D. Stenolen, J.H. Resau, N.G. Copeland, and N.A. Jenkins. 1999. Direct interaction of microtubule- and actin-based transport motors. *Nature.* 397:267–270.

Kacza, J., W. Hartig, and J. Seeger. 1997. Oxygen-enriched photoconversion of fluorescent dyes by means of a closed conversion chamber. *J. Neurosci. Methods.* 71:225–232.

Kreis, T. 1987. Microtubules containing detyrosinated tubulin are less dynamic. *EMBO (Eur. Mol. Biol. Organ.) J.* 6:2597–2606.

Kuznetsov, S.A., G.M. Langford, and D.G. Weiss. 1992. Actin-dependent organelle movement in squid axoplasm. *Nature.* 356:722–725.

Langford, G.M. 1995. Actin- and microtubule-dependent organelle motors: interrelationship between the two motility systems. *Curr. Opin. Cell Biol.* 7:82–88.

Lewis, A.K., and P.C. Bridgman. 1996. Mammalian myosin 1 α is concentrated near the plasma membrane in nerve growth cones. *Cell Motil. Cytoskelet.* 33: 130–150.

Lubke, J. 1993. Photoconversion of diaminobenzidine with different fluorescent neuronal markers into a light and electron microscopic dense reaction product. *Microsc. Res. Tech.* 24:2–14.

Marsh, L., and P.C. Letourneau. 1984. Growth of neurites without filopodial or lamellipodial activity in the presence of cytochalasin B. *J. Cell Biol.* 99:2041–2047.

Mercer, J.A., P.K. Seperack, M.C. Strobel, N.G. Copeland, and N.A. Jenkins. 1991. Novel myosin heavy chain encoded by murine dilute coat colour locus. *Nature.* 349:709–713.

Morris, R.L., and P.J. Hollenbeck. 1995. Axonal transport of mitochondria along microtubules and F-actin in living vertebrate neurons. *J. Cell Biol.* 131:

1315–1326.

Mrini, A., H. Moukhles, H. Jacomy, O. Bosler, and G. Doucet. 1995. Efficient immunodetection of various protein antigens in glutaraldehyde-fixed brain tissue. *J. Histochem. Cytochem*. 43:1285–1291.

Nakata, T., S. Terada, and N. Hirokawa. 1998. Visualization of the dynamics of synaptic vesicle and plasma membrane proteins in living axons. *J. Cell Biol*. 140:659–674.

Nascimento, A.A.C., R.G. Amaral, R.E. Bizario, R.E. Larson, and E.M. Espreafico. 1997. Subcellular localization of myosin-V in the B16 melanoma cells, a wild–type cell line for the dilute gene. *Mol. Biol. Cell.* 8:1971–1988.

Okada, Y., H. Yamazaki, Y. Sekine-Aizawa, and N. Hirokawa. 1995. The neuron-specific kinesin superfamily protein KIF1A is a unique monomeric motor for anterograde axonal transport of synaptic vesicle precursors. *Cell.* 81: 769–780.

Prekaris, R., and D.M. Terrian. 1997. Brain myosin V is a synaptic vesicle–associated motor protein: evidence for a Ca^{2+}-dependent interaction with the synaptobrevin–synaptophysin complex. *J. Cell Biol.* 137:1589–1601.

Provance, D., M. Wei, V. Ipe, and J. Mercer. 1996. Cultured melanocytes from dilute mutant mice exhibit dendritic morphology and altered melanosome distribution. *Proc. Natl. Acad. Sci. USA*. 93:14554–14558.

Reck-Peterson, S.L., P.J. Novick, and M.S. Mooseker. 1999. The tail of a yeast class V myosin, myo2p, functions as a localization domain. *Mol. Biol. Cell.* 10:1001–1017.

Rogers, S.L., and V.I. Gelfand. 1998. Myosin cooperates with microtubule motors during organelle transport in melanophores. *Curr. Biol*. 8:161–164.

Schulze, E., D.J. Asai, J.C. Bulinski, and M. Kirschner. 1987. Post-translational modification and microtubule stability. *J. Cell Biol.* 105:2167–2177.

Spector, I., N.R. Shochet, D. Balsberger, and Y. Kashman. 1989. Latrunculins-novel marine macrolides that disrupt microfilament organization and affect cell growth: I. Comparison with cytochalasin. *Cell Motil. Cytoskelet.* 13:127–144.

Strobel, M.C., P.K. Seperack, N.G. Copeland, and N.A. Jenkins. 1990. Molecular analysis of two mouse dilute locus deletion mutations: spontaneous dilute lethal 20J and radiation-induced dilute prenatal lethal Aa2 alleles. *Mol. Cell Biol.* 10:501–509.

Tabb, J.S., B.J. Molyneaux, D.L. Cohen, S.A. Kuznetsov, and G.M. Langford. 1998. Transport of ER vesicles on actin filaments in neurons by myosin V. *J. Cell Sci.* 111:3221–3234.

Takagishi, Y., S.-i. Oda, S. Hayasaka, K. Dekker-Ohno, T. Shikata, M. Inouye, and H. Yamamura. 1996. The dilute-lethal (d^l) gene attacks a Ca^{2+} store in the dendritic spine of Purkinje cells in mice. *Neurosci. Lett.* 215:169–172.

Wei, Q., X. Wu, and J.A. Hammer III. 1997. The predominant defect in dilute melanocytes is in melanosome distribution and not cell shape, supporting a role for myosin V in melanosome transport. *J. Muscle Res. Cell Motil.* 18: 517–527.

Wolenski, J.S., R.E. Cheney, M.S. Mooseker, and P. Forscher. 1995. In vitro motility of immunoadsorbed brain myosin V using limulus acrosomal process and optical tweezer-based assay. *J. Cell Sci.* 108:1489–1496.

Wu, X., B. Bowers, Q. Wei, B. Kocher, and J.A. Hammer III. 1997. Myosin V associates with melanosomes in mouse melanocytes: evidence that myosin V is an organelle motor. *J. Cell Sci.* 110:847–859.

Wu, X., B. Bowers, K. Rao, Q. Wei, and J.A. Hammer III. 1998. Visualization of melanosome dynamics within wild-type and dilute melanocytes suggests a paradigm for myosin V function in vivo. *J. Cell Biol.* 143:1899–1918.

Yonekawa, Y., A. Harada, Y. Okada, T. Furrakoshi, Y. Kanai, Y. Takei, S. Terada, T. Noda, and N. Hirokawa. 1998. Defect in synaptic vesicle precursor transport and neuronal cell death in KIF1A motor protein-deficient mice. *J. Cell Biol.* 141:431–441.

Ziv, N.E., and S.J. Smith. 1996. Evidence for a role of dendritic filopodia in synaptogenesis and spine formation. *Neuron*. 17:91–102.